Arch Appl Mech (2015) 85:1459–1468
DOI 10.1007/s00419-014-0945-8

SPECIAL

Regina Schmitt · Charlotte Kuhn · Robert Skorupski · Marek Smaga · Dietmar Eifler · Ralf Müller

A combined phase field approach for martensitic transformations and damage

Received: 23 December 2013 / Accepted: 3 June 2014 / Published online: 29 November 2014

Abstract A combined continuum phase field model for martensitic transformations and fracture is introduced. The positive volume change that accompanies the phase transformation from austenite to martensite leads to an eigenstrain within the martensitic phase, which is considered within the present approach. Since the eigenstrain leads to both tensile and compressive loads, the model accounts for the sign of the local volume change. With aid of this model, the interactions between microcrack propagation and the formation of the martensitic phase are studied in two dimensions. Martensite forms in agreement with experimental observations at the crack tip and thus influences the crack formation. The numerical implementation is performed with finite elements. For the transient terms, an implicit time integration scheme is employed.

Keywords Phase field model · Phase transformation · Continuum fracture model · Crack propagation · Finite elements

1 Introduction

The microstructure evolution of metastable austenitic steels results from the complex interplay of different processes on the microlevel. One crucial phenomenon is the martensitic transformation, during which the crystal lattice changes from the austenitic to the α'-martensitic phase. The phase transformation is accompanied by a positive volume change plus a lattice shear, which leads to an eigenstrain or transformation strain within the martensitic phase. In conjunction with damage and fatigue behavior on the microscale, α'-martensite mainly forms at the crack tip (see, e.g. [1–5]). This influences the crack propagation due to the eigenstrain acting in the α'-martensite. On the other hand, the formation of the α'-phase is affected by crack growth. To study these interactions, a combined phase field model for martensitic transformations and crack propagation is introduced in this work.

A continuum fracture model is proposed in [6] as a variational formulation of brittle fracture, where the total energy is minimized with respect to the crack geometry and the displacement field. However, in the

R. Schmitt (✉) · R. Müller
Institute of Applied Mechanics, University of Kaiserslautern, P.O. Box 3049, 67653 Kaiserslautern, Germany
E-mail: rschmitt@rhrk.uni-kl.de
Tel.: +631-205-2125

C. Kuhn
Computational Mechanics, University of Kaiserslautern, P.O. Box 3049, 67653 Kaiserslautern, Germany
Tel.: +631-205-2125

R. Skorupski · M. Smaga · D. Eifler
Institute of Materials Science and Engineering, University of Kaiserslautern, P.O. Box 3049, 67653 Kaiserslautern, Germany
Tel.: +49 631-205-2411

presence of cracks, the numerical discretization is due to the discontinuous displacement field cumbersome. These numerical difficulties can be overcome by a regularized approximation of the model, e.g. [7–9]. For the regularization of the energy of fracture, a damage variable s is introduced describing crack formation and growth. In this work, $s = 1$ indicates unbroken material, and $s = 0$ represents a crack.

To consider the martensitic transformation in the intact material, an order parameter c is introduced, indicating the present phase. In this regard, several authors have studied phase field models for martensitic transformations, e.g. [10–18].

The consideration of crystalline damage and martensitic transformations is studied in [19]. The authors propose a thermomechanical model, where the volume fractions of the phases and damaged volume are taken into account. In [20], Garion and coworkers use a combined model for phase transformation and damage to examine the evolution of the volume fractions of both martensite and damage, which are related to the plastic strain at cryogenic temperatures. A combined phase field approach is applied in [21], where a damage variable is coupled with a phase field for ferroelectrics. In this work, a similar ansatz is applied: A combined phase field potential is formulated that resembles for $s = 1$ the phase field potential for martensitic transformations proposed in [22,23], taking into account the transformation-induced eigenstrain as a function of the order parameter. Since the eigenstrain in the martensitic phase induces both compressive and tensile stresses, the sign of the local volume change is considered and the compressive part is not affected by the crack field, according to [24–26]. An alternative ansatz, based on a spectral decomposition of the strain tensor $\boldsymbol{\varepsilon}$, is proposed in [27].

With aid of the model introduced in this work, the interactions between crack propagation and martensitic transformations are examined in a 2D plane strain setting. Therefore, an austenitic specimen with preexisting crack under mode I loading is studied, where the transformation strain plays a crucial role. For the numerical realization, finite elements together with an implicit time integration scheme are used.

2 A combined phase field approach for martensitic transformations and damage evolution

A combined phase field approach for martensitic transformations and damage evolution is proposed. Therefore, a damage variable s is introduced to indicate the crack situation. For $s = 1$, the material is undamaged while $s = 0$ represents a crack. The combined phase field energy expression π is given as follows, see [7–9,21],

$$\pi = \underbrace{s^2\,\psi_s + \psi_{ns} + (1 - s^2)\,\eta}_{\pi^{\text{bulk}}} + \underbrace{\frac{G_s}{4L_s}(1 - s)^2 + G_s\,L_s||\nabla s||^2}_{\pi^{\text{crack}}}. \tag{1}$$

In (1), π consists of two parts: the bulk energy π^{bulk} and the fracture energy π^{crack}. In the bulk energy, ψ_s and ψ_{ns} account for the phase field potential of the undamaged solid subject to martensitic transformations, where only ψ_s is coupled with the damage variable s. Details are discussed in subsection 2.1. The third term of (1), $(1 - s^2)\,\eta$ with $0 < \eta \ll 1$ is introduced to retain a residual stiffness if $s = 0$. Thus, for undamaged material ($s = 1$), the bulk energy π^{bulk} equals the phase field potential for martensitic transformations $\psi = \psi_s + \psi_{ns}$. If there is a crack ($s = 0$), only the residual stiffness η and the uncoupled part ψ_{ns} remain.

The second part of (1) represents the fracture energy π^{crack}. According to existing theories on phase field models for fracture (see, e.g. [9]), it depends on the damage parameter s and its gradient ∇s. The width of the transition zone between undamaged and broken material is controlled by the parameter L_s while G_s stands for the crack resistance, which can be expressed by the fracture toughness.

Furthermore, the temporal evolution of the damage parameter s is assumed to be proportional to the variational derivative of the combined phase field potential π with respect to s, which is known as the time-dependent Ginzburg-Landau equation (TDGL)

$$\dot{s} = -M_s\frac{\delta\pi}{\delta s} = -M_s\left[2\,s\,(\psi_s - \eta) - \frac{G_s}{2\,L_s}(1 - s) - 2\,G_s\,L_s\,\Delta s\right]. \tag{2}$$

In (2), M_s is the mobility parameter, scaling the kinetics of the fracture process. A more detailed discussion of a continuum phase field model for fracture can be found in [9].

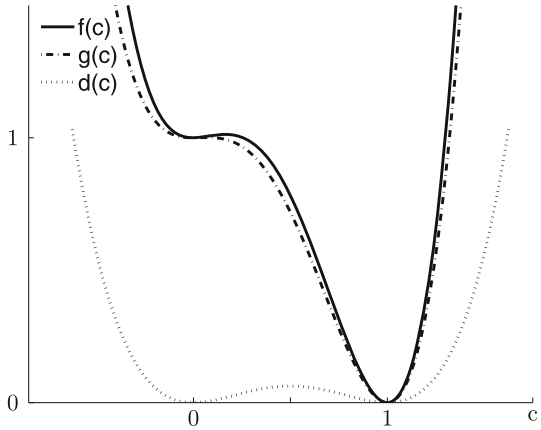

Fig. 1 Plot of the Landau polynomial expansion $f(c)$ (*solid line*) split up into the symmetric double well $d(c)$ (*dotted line*) and the asymmetric part $g(c)$ (*dash-dotted line*)

2.1 Phase field potential for martensitic transformations

During the martensitic transformation, the crystal lattice of the undamaged solid changes from the metastable phase austenite to the stable phase α'-martensite. In this work, a phase field approach for martensitic transformations introduced in [22,23] is applied, where an order parameter c indicates the present phase: $c = 0$ for austenite and $c = 1$ for α'-martensite. The phase field potential for martensitic transformations ψ consists of three parts: the elastic energy density W, the gradient energy density ψ^{grad} and the separation potential ψ^{sep}

$$\begin{aligned}\psi(\boldsymbol{\varepsilon}, c, \boldsymbol{\nabla} c) &= W(\boldsymbol{\varepsilon}, c) + \psi^{\text{grad}}(\boldsymbol{\nabla} c) + \psi^{\text{sep}}(c) \\ &= W(\boldsymbol{\varepsilon}, c) + \frac{1}{2}\kappa_{\text{grad}} G\, L ||\boldsymbol{\nabla} c||^2 + \kappa_{\text{sep}} \frac{G}{L} f(c). \end{aligned} \tag{3}$$

According to [28], the proper choice for the calibration constants κ_{grad} and κ_{sep} results in G corresponding to the specific energy density while the parameter L controls the width of the transition zone. The function $f(c)$, which appears in the separation potential ψ^{sep}, is a Landau polynomial expansion $f(c) = 1 + \frac{\mathscr{A}}{2}c^2 - \frac{\mathscr{B}}{3}c^3 + \frac{\mathscr{C}}{4}c^4$, with $\mathscr{B} = 3\,\mathscr{A} + 12$ and $\mathscr{C} = 2\,\mathscr{A} + 12$ (see [15]). The plot of $f(c)$ (solid line in Fig. 1) shows that the function has a local minimum $f(c) = 1$ for $c = 0$, which corresponds to the metastable austenitic phase and a global minimum $f(c) = 0$ for $c = 1$ corresponding to the stable martensitic phase. However, this asymmetric function leads to difficulties when the phase field model for martensitic transformations is combined with the damage model. Due to its higher separation energy, a crack in the austenitic phase would be more likely than in martensite. Therefore, the separation potential is split into the symmetric double well part with $d(c) = c^2(1-c)^2$ (dotted line in Fig. 1) and the asymmetric part $g(c) = \mathscr{D} + \mathscr{E}\,c^2 + \mathscr{F}\,c^3 + \mathscr{G}\,c^4$, which is plotted with a dash-dotted line in Fig. 1. Thus, ψ^{sep} can be written as

$$\psi^{\text{sep}} = \psi_d^{\text{sep}} + \psi_g^{\text{sep}} = \kappa_{\text{sep}} \frac{G}{L} d(c) + \kappa_{\text{sep}} \frac{G}{L} g(c), \tag{4}$$

where only the symmetric part ψ_d^{sep} is coupled with the damage parameter. The asymmetric function $g(c)$ should possess the same extrema as $f(c)$, which leads to $\mathscr{D} = 1$, $\mathscr{E} = \mathscr{G} - 3$, $\mathscr{F} = 2 - 2\,\mathscr{G}$ and $\mathscr{G} > 3$. The elastic energy $W(\boldsymbol{\varepsilon}, c)$ in (3) is defined as

$$W(\boldsymbol{\varepsilon}, c) = \frac{1}{2}\left[\boldsymbol{\varepsilon} - \boldsymbol{\varepsilon}^0(c)\right] : \mathbb{C}(c)\left[\boldsymbol{\varepsilon} - \boldsymbol{\varepsilon}^0(c)\right], \tag{5}$$

where for the 2D analysis in this work, plane strain conditions are assumed. In (5), $\boldsymbol{\varepsilon} = \frac{1}{2}\left(\boldsymbol{\nabla}\boldsymbol{u} + \boldsymbol{\nabla}^T\boldsymbol{u}\right)$ is the linearized strain tensor; the elastic stiffness tensor and the eigenstrain tensor depend linearly on the order parameter c

$$\mathbb{C}(c) = \mathbb{C}_{\text{A}} + c\,(\mathbb{C}_{\text{M}} - \mathbb{C}_{\text{A}})\,, \quad \boldsymbol{\varepsilon}^0(c) = c\,\boldsymbol{\varepsilon}^0 \quad \text{with} \quad \boldsymbol{\varepsilon}^0 = \begin{bmatrix} \varepsilon^0_{\text{vol}} & \varepsilon^0_{12} \\ \varepsilon^0_{12} & \varepsilon^0_{\text{vol}} \end{bmatrix}. \tag{6}$$

The martensitic transformation is accompanied by a positive volume change (see, e.g. [1]), which is considered by the diagonal entries $\varepsilon^0_{\text{vol}}$ in the eigenstrain tensor $\boldsymbol{\varepsilon}^0$, while ε^0_{12} accounts for the lattice shear. To combine this model for martensitic transformations with the damage model, the elastic energy is split up into a volumetric W^{vol} and a deviatoric part W^{dev}. Additionally, the sign of the local volume change is taken into account (see [24–26]),

$$W = W^{\text{vol}-} + W^{\text{vol}+} + W^{\text{dev}}, \tag{7}$$

where

$$W^{\text{vol}-} = \begin{cases} \dfrac{K(c)}{2}\,\text{tr}(\boldsymbol{\varepsilon} - \boldsymbol{\varepsilon}^0(c))^2 & \text{if} \quad \text{tr}(\boldsymbol{\varepsilon} - \boldsymbol{\varepsilon}^0(c)) < 0 \\ 0 & \text{else} \end{cases}, \tag{8}$$

$$W^{\text{vol}+} = \begin{cases} \dfrac{K(c)}{2}\,\text{tr}(\boldsymbol{\varepsilon} - \boldsymbol{\varepsilon}^0(c))^2 & \text{if} \quad \text{tr}(\boldsymbol{\varepsilon} - \boldsymbol{\varepsilon}^0(c)) \geq 0 \\ 0 & \text{else} \end{cases} \tag{9}$$

and

$$W^{\text{dev}} = \mu(c)\left[\boldsymbol{e} - c\,\boldsymbol{e}^0\right] : \left[\boldsymbol{e} - c\,\boldsymbol{e}^0\right]. \tag{10}$$

In (10), $\boldsymbol{e} = \boldsymbol{\varepsilon} - \dfrac{\text{tr}(\boldsymbol{\varepsilon})}{2}\,\mathbf{1}$ and $\boldsymbol{e}^0 = \boldsymbol{\varepsilon}^0 - \dfrac{\text{tr}(\boldsymbol{\varepsilon}^0)}{2}\,\mathbf{1}$ are the deviatoric parts of the strain tensor $\boldsymbol{\varepsilon}$ and the eigenstrain tensor $\boldsymbol{\varepsilon}^0$ in this 2D formulation, with $\mathbf{1}$ denoting the 2D identity tensor. Furthermore, $K(c)$ and $\mu(c)$ are the bulk and the shear modulus, respectively, depending on the phase transformation order parameter c. This decomposition of the elastic energy W requires the elasticity tensors $\mathbb{C}_A$ and $\mathbb{C}_M$ to be isotropic, which implies $K(c) = K_A + c\,(K_M - K_A)$ and $\mu(c) = \mu_A + c\,(\mu_M - \mu_A)$.

Thus, the phase field potential for martensitic transformations ψ can be split up in the following way

$$\psi = \psi_s + \psi_{ns}, \tag{11}$$

$$\psi_s = \underbrace{W^{\text{vol}+} + W^{\text{dev}} + \psi_d^{\text{sep}}}_{\psi^*} + \psi^{\text{grad}} = \psi^* + \psi^{\text{grad}}, \tag{12}$$

$$\psi_{ns} = W^{\text{vol}-} + \psi_g^{\text{sep}}. \tag{13}$$

In (1), ψ_{ns} is not coupled with the damage variable s. In that way, the elastic energy associated to the negative volume change $W^{\text{vol}-}$ cannot be minimized by creating cracks, which leads to asymmetric results in tension and compression [24–26]. This distinction is necessary since the eigenstrain $\boldsymbol{\varepsilon}^0(c)$ of the martensitic phase leads to compression even if exclusively traction load is applied. Additionally, the interaction of the asymmetric part of the separation potential ψ_g^{sep} with the crack energy π_{crack} is prevented. A coupling of ψ_g^{sep} with the damage variable would lead to unphysical results.

Different from the approach in [22,23], the evolution equation of the order parameter c is given by the variational derivative of the combined phase field potential π (instead of the phase field potential for martensitic transformations ψ) with respect to the order parameter c, i.e.,

$$\begin{aligned} \dot{c} &= -M\frac{\delta\pi}{\delta c} = -M\left[s^2\frac{\delta\psi_s}{\delta c} + \frac{\delta\psi_{ns}}{\delta c}\right] \\ &= -M\left[s^2\left(\frac{\partial W^{\text{vol}+}}{\partial c} + \frac{\partial W^{\text{dev}}}{\partial c} + \kappa_{\text{sep}}\frac{G}{L}\frac{\partial d}{\partial c} - \kappa_{\text{grad}}\,G\,L\,\Delta c\right)\right. \\ &\quad \left. + \frac{\partial W^{\text{vol}-}}{\partial c} + \kappa_{\text{sep}}\frac{G}{L}\frac{\partial g}{\partial c}\right]. \end{aligned} \tag{14}$$

The mobility parameter M influences the velocity of the martensitic transformation. Thus, the martensitic phase evolves in dependence of the damage variable s, considering the influence of crack propagation on the martensitic transformation.

2.2 Field equations

Neglecting inertia effects, the balance of linear momentum states

$$\operatorname{div}\boldsymbol{\sigma} + \boldsymbol{f} = \boldsymbol{0}, \tag{15}$$

where the volume force $\boldsymbol{f}$ is assumed to be $\boldsymbol{f} = \boldsymbol{0}$. In (15), the Cauchy stress tensor $\boldsymbol{\sigma}$ is given by the constitutive relation

$$\boldsymbol{\sigma} = \frac{\partial \pi}{\partial \boldsymbol{\varepsilon}} = K(c)\,\mathrm{tr}^{-}(\boldsymbol{\varepsilon} - \boldsymbol{\varepsilon}^0(c))\boldsymbol{1} + s^2\left[K(c)\mathrm{tr}^{+}(\boldsymbol{\varepsilon} - \boldsymbol{\varepsilon}^0(c))\boldsymbol{1} + 2\,\mu(c)\left(\boldsymbol{e} - c\,\boldsymbol{e}^0\right)\right]. \tag{16}$$

The evolution Eq. (2) and (14), for the damage variable s and the order parameter c, respectively, plus the equilibrium condition (15) complete the set of field equations.

3 Numerical implementation

The model is implemented in a 2D finite element framework, applying an implicit time integration scheme for the transient terms. The nodal degrees of freedom are the mechanical displacements $\boldsymbol{u}$, the order parameter c and the damage variable s. The numerical implementation is explained in detail in [29]. For the implementation, the weak formulations of the field Eqs. (15), (14) and (2) are discretized

$$\int_V \nabla\boldsymbol{\eta}_u : \boldsymbol{\sigma}\,\mathrm{d}V = \int_{\partial V_t} \boldsymbol{\eta}_u \boldsymbol{t}^*\,\mathrm{d}A, \tag{17}$$

$$\int_V \frac{\dot{c}}{M}\eta_c\,\mathrm{d}V - \int_V s^2\,\boldsymbol{q}\,\nabla\eta_c\,\mathrm{d}V + \int_V s^2\,\frac{\partial\psi^*}{\partial c}\,\eta_c\,\mathrm{d}V + \int_V \frac{\partial\psi_{ns}}{\partial c}\,\eta_c\,\mathrm{d}V = -\int_{\partial V} q^*\,\eta_c\,\mathrm{d}A, \tag{18}$$

and

$$\int_V \frac{\dot{s}}{M_s}\eta_s\,\mathrm{d}V - \int_V \boldsymbol{q}_s\,\nabla\eta_s\,\mathrm{d}V + \int_V \frac{\partial\pi}{\partial s}\,\eta_s\,\mathrm{d}V = -\int_{\partial V} q_s^*\,\eta_s\,\mathrm{d}A, \tag{19}$$

where $\boldsymbol{\eta}_u$, η_c and η_s are test functions for the respective field quantities while $\boldsymbol{q} = -\kappa_{\mathrm{grad}}\,G\,L\,\nabla c$ and $\boldsymbol{q}_s = -G_s\,L_s\,\nabla s$. The boundary conditions for the stresses $\boldsymbol{\sigma}$ is the traction $\boldsymbol{t}^* = \boldsymbol{\sigma}\,\boldsymbol{n}$, for $\boldsymbol{q}$ the normal flux $\boldsymbol{q}\cdot\boldsymbol{n} = 0$ and for $\boldsymbol{q}_s$ the normal flux $\boldsymbol{q}_s\cdot\boldsymbol{n} = 0$, where $\boldsymbol{n}$ is the outer normal vector to the volume V. For the discretization of $\boldsymbol{u}$, c and s, the shape functions N_I for node I are used while Voigt notation is denoted by an underbar $\underline{(\cdot)}$ and nodal quantities by the superimposed hat $\hat{(\cdot)}$

$$\underline{\boldsymbol{u}} = \sum_{I=1}^{N} N_I\,\hat{\underline{\boldsymbol{u}}}_I, \qquad \underline{\boldsymbol{\varepsilon}} = \sum_{I=1}^{N} \underline{\boldsymbol{B}}_I^u\,\hat{\underline{\boldsymbol{u}}}_I, \tag{20}$$

$$c = \sum_{I=1}^{N} N_I\,\hat{c}_I, \qquad \underline{\nabla c} = \sum_{I=1}^{N} \underline{\boldsymbol{B}}_I^c\,\hat{c}_I, \tag{21}$$

$$s = \sum_{I=1}^{N} N_I\,\hat{s}_I, \qquad \underline{\nabla s} = \sum_{I=1}^{N} \underline{\boldsymbol{B}}_I^s\,\hat{s}_I, \tag{22}$$

$$\dot{c} = \sum_{I=1}^{N} N_I\,\hat{\dot{c}}_I, \qquad \dot{s} = \sum_{I=1}^{N} N_I\,\hat{\dot{s}}_I, \tag{23}$$

where

$$\underline{\boldsymbol{B}}_I^u = \begin{bmatrix} N_{I,x} & 0 \\ 0 & N_{I,y} \\ N_{I,y} & N_{I,x} \end{bmatrix}, \quad \underline{\boldsymbol{B}}_I^c = \begin{bmatrix} N_{I,x} \\ N_{I,y} \end{bmatrix} \quad \text{and} \quad \underline{\boldsymbol{B}}_I^s = \begin{bmatrix} N_{I,x} \\ N_{I,y} \end{bmatrix}. \tag{24}$$

The discretizations (20–23) are applied to the left-hand sides of Eqs. (17), (18) and (19) to obtain the nodal residuals as a function of the nodal degrees of freedom $\hat{\underline{\boldsymbol{d}}}_J = (\hat{\underline{\boldsymbol{u}}}_J, \hat{c}_J, \hat{s}_J)^T$ and the rates $\dot{\hat{\underline{\boldsymbol{d}}}}_J$,

$$\underline{\boldsymbol{R}}_I(\hat{\underline{\boldsymbol{d}}}_J, \dot{\hat{\underline{\boldsymbol{d}}}}_J) = \begin{bmatrix} \underline{\boldsymbol{R}}^u_I(\hat{\underline{\boldsymbol{d}}}_J) \\ R^c_I(\hat{\underline{\boldsymbol{d}}}_J, \dot{\hat{\underline{\boldsymbol{d}}}}_J) \\ R^s_I(\hat{\underline{\boldsymbol{d}}}_J, \dot{\hat{\underline{\boldsymbol{d}}}}_J) \end{bmatrix} \tag{25}$$

$$= \begin{bmatrix} \displaystyle\int_V \left(\underline{\boldsymbol{B}}^u_I\right)^T \underline{\boldsymbol{\sigma}}\, \mathrm{d}V \\ \displaystyle\int_V N_I \frac{\dot{c}}{M}\, \mathrm{d}V - \int_V \left(\underline{\boldsymbol{B}}^c_I\right)^T s^2\, \boldsymbol{q}\, \mathrm{d}V + \int_V N_I \left(s^2 \frac{\partial \psi^*}{\partial c} + \frac{\partial \psi_{ns}}{\partial c}\right) \mathrm{d}V \\ \displaystyle\int_V N_I \frac{\dot{s}}{M_s}\, \mathrm{d}V - \int_V \left(\underline{\boldsymbol{B}}^s_I\right)^T \boldsymbol{q}_s\, \mathrm{d}V + \int_V N_I \frac{\partial \pi}{\partial s}\, \mathrm{d}V \end{bmatrix}.$$

The derivative of the nodal residuals with respect to the nodal degrees of freedom yields the entries of the stiffness matrix $\underline{\boldsymbol{K}}_{IJ}$ given by

$$\underline{\boldsymbol{K}}_{IJ} = \frac{\partial \underline{\boldsymbol{R}}_I}{\partial \hat{\underline{\boldsymbol{d}}}_J} = \begin{bmatrix} \underline{\boldsymbol{K}}^{uu}_{IJ} & \underline{\boldsymbol{K}}^{uc}_{IJ} & \underline{\boldsymbol{K}}^{us}_{IJ} \\ \underline{\boldsymbol{K}}^{cu}_{IJ} & \underline{\boldsymbol{K}}^{cc}_{IJ} & \underline{\boldsymbol{K}}^{cs}_{IJ} \\ \underline{\boldsymbol{K}}^{su}_{IJ} & \underline{\boldsymbol{K}}^{sc}_{IJ} & \underline{\boldsymbol{K}}^{ss}_{IJ} \end{bmatrix}, \tag{26}$$

with

$$\underline{\boldsymbol{K}}^{uu}_{IJ} = \int_V \left(\underline{\boldsymbol{B}}^u_I\right)^T \frac{\partial}{\partial \hat{\underline{\boldsymbol{u}}}} \left(\frac{\partial \pi}{\partial \underline{\boldsymbol{\varepsilon}}}\right) \mathrm{d}V$$

$$\underline{\boldsymbol{K}}^{uc}_{IJ} = \underline{\boldsymbol{K}}^{cu}_{IJ} = \int_V \left(\underline{\boldsymbol{B}}^u_I\right)^T s^2 \left(\tilde{\underline{\boldsymbol{\sigma}}} - \underline{\boldsymbol{\sigma}}^0\right) N_J\, \mathrm{d}V$$

$$\underline{\boldsymbol{K}}^{us}_{IJ} = \underline{\boldsymbol{K}}^{su}_{IJ} = \int_V \left(\underline{\boldsymbol{B}}^u_I\right)^T \frac{\partial W}{\partial s} N_J\, \mathrm{d}V$$

$$\underline{\boldsymbol{K}}^{cc}_{IJ} = \int_V \left[s^2 \kappa_{\mathrm{grad}} GL \left(\underline{\boldsymbol{B}}^c_I\right)^T \underline{\boldsymbol{B}}^c_J + N_I \left(s^2 \frac{\partial^2 \psi^*}{\partial c^2} + \frac{\partial^2 \psi_{ns}}{\partial^2 c^2}\right) N_J\right] \mathrm{d}V$$

$$\underline{\boldsymbol{K}}^{cs}_{IJ} = \underline{\boldsymbol{K}}^{sc}_{IJ} = \int_V 2\, s \left[N_I \frac{\partial \psi^*}{\partial c} - \left(\underline{\boldsymbol{B}}^s_I\right)^T \boldsymbol{q}\right] N_J\, \mathrm{d}V$$

$$\underline{\boldsymbol{K}}^{ss}_{IJ} = \int_V \left[G_s L_s \left(\underline{\boldsymbol{B}}^s_I\right)^T \underline{\boldsymbol{B}}^s_J + N_I \frac{\partial^2 \pi}{\partial s^2} N_J\right] \mathrm{d}V$$

where $\tilde{\underline{\boldsymbol{\sigma}}} = \left(\underline{\mathbb{C}}_M - \underline{\mathbb{C}}_A\right)\left(\underline{\boldsymbol{\varepsilon}} - \underline{\boldsymbol{\varepsilon}}^0(c)\right)$ and $\underline{\boldsymbol{\sigma}}^0 = \underline{\mathbb{C}}(c)\, \dfrac{\partial \underline{\boldsymbol{\varepsilon}}^0(c)}{\partial c}$.
Furthermore, the damping matrix $\underline{\boldsymbol{D}}_{IJ}$ reads

$$\underline{\boldsymbol{D}}_{IJ} = \frac{\partial \underline{\boldsymbol{R}}_I}{\partial \dot{\hat{\underline{\boldsymbol{d}}}}_J} = \int_V \begin{bmatrix} 0 & 0 & 0 \\ 0 & \dfrac{1}{M} N_I^2 & 0 \\ 0 & 0 & \dfrac{1}{M_s} N_I^2 \end{bmatrix} \mathrm{d}V. \tag{27}$$

The integrals are evaluated using Gauß quadrature. Applying the backward Euler method as an implicit time integration scheme (see, e.g. [30]), the system matrix $\underline{\boldsymbol{S}}_{IJ}$ is formed according to

$$\underline{\boldsymbol{S}}_{IJ} = \frac{1}{\Delta t}\, \underline{\boldsymbol{D}}_{IJ} + \underline{\boldsymbol{K}}_{IJ}. \tag{28}$$

Within the global Newton iteration, $\underline{\boldsymbol{S}}_{IJ}$ is used to compute the increments of $\hat{\underline{\boldsymbol{d}}}_J$ for the new time step.

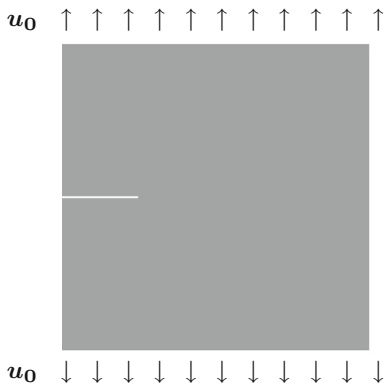

Fig. 2 Inital configuration: austenitic specimen with preexisting crack under mode I loading

4 Numerical examples

The model is implemented into a four-node quadrilateral plane element with bilinear shape functions. Concerning the material parameters, the bulk and shear moduli

$$\begin{aligned} K_{\mathrm{A}} &= 1.027\,10^5 \frac{\mathrm{N}}{\mathrm{mm}^2}, & \mu_{\mathrm{A}} &= 0.28\,10^5 \frac{\mathrm{N}}{\mathrm{mm}^2}, \\ K_{\mathrm{M}} &= 1.1\,K_{\mathrm{A}}, & \mu_{\mathrm{M}} &= 1.1\,\mu_{\mathrm{A}}, \end{aligned} \tag{29}$$

are taken into account, where K_{A} and μ_{A} are proposed in [15]. The eigenstrain is set to

$$\underline{\boldsymbol{\varepsilon}}^0 = \left[0.02\ 0.02\ 0.1\right]^T \tag{30}$$

which considers the volume change and the lattice shear during the martensitic transformation. The calibration constants are determined to be $\kappa_{\mathrm{sep}} = 3.2937$ and $\kappa_{\mathrm{grad}} = 1.5$, leading to the interface energy density between the phases corresponding to $G = 0.1\,\frac{\mathrm{J}}{\mathrm{m}^2}$. The length parameter is set to $L = 5\,\mathrm{nm}$, so that the transition zone can be resolved by several elements. Furthermore, for the crack energy $G_s = 0.2\,\frac{\mathrm{J}}{\mathrm{m}^2}$ and the crack width $L_s = 5\,\mathrm{nm}$ are taken into account. The value of the mobility constant $M_s = 1.0 \cdot 10^{12}\,\frac{\mathrm{m}^3}{\mathrm{Js}}$ is chosen fairly high, so that the crack solution can be considered as quasi-static. In order to relate the phase transformation to the same time scale, the mobility constant $M = 1.0 \cdot 10^{12}\,\frac{\mathrm{m}^3}{\mathrm{Js}}$ is used for evolution of the martensitic phase.

In the following, two examples with the same initial configuration are studied, which can be seen in Fig. 2: An austenitic specimen with a preexisting crack under mode I loading.

4.1 Purely austenitic specimen

For comparison, in a first example, the martensitic transformation is suppressed by imposing Dirichlet boundary conditions $c = 0$ on the order parameter c. The resulting contour plots can be seen in Fig. 3, where elements with $s < 0.1$ are suppressed. Under the load applied, the crack starts to grow and propagates straight through the austenitic matrix. This result is expectable since the material of the specimen is homogeneous.

4.2 Specimen subject to phase transformation

In this example, again an austenitic specimen is examined and however subject to the martensitic transformation. In Fig. 4, the martensitic evolution can be seen, where austenite and α'-martensite are depicted in black and white, respectively. Under mode I loading, α'-martensite forms at the crack tip (Fig. 4a), in agreement with experimental studies [1,4]. In the following time steps, the martensitic phase evolves in a plate-like shape in diagonal direction (Fig. 4b), confirmed by other theoretical studies, e.g. [15,22], and crystallographic theories [31]. In [32], it is shown that the diagonal growing direction results from the volumetric part of the

(a) **(b)**

Fig. 3 Crack formation for an austenitic specimen with preexisting crack under mode I loading. **a** $t = 1.5\,10^{-7}$. **b** $t = 4.34\,10^{-7}$

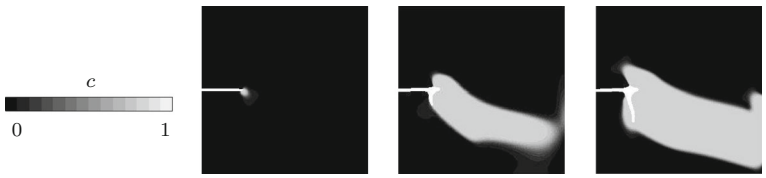

(a) **(b)** **(c)**

Fig. 4 Austenitic specimen (*black*) with preexisting crack under mode I loading: evolution of the martensitic phase (*white*). **a** $t = 1.5\,10^{-7}$. **b** $t = 2.17\,10^{-7}$. **c** $t = 2.45\,10^{-7}$

transformation-induced eigenstrain. In comparison with the austenitic specimen in subsection 4.1, a different crack pattern is observed (Fig. 4c). Thus, the formation of the martensitic phase influences the crack evolution. Fig. 5b, d show the distribution of the normal stress component in vertical direction σ_{yy} for both simulations after a few time steps, where tensile stresses are shown in white, compressive stresses in black. The stress distribution for the purely austenitic specimen in Fig. 5b is expected since high tensile normal stresses in vertical direction arise at the crack tip. However, the formation of martensite at the crack tip (Fig. 5c) leads to a different stress field (Fig. 5d). The positive volume change, which accompanies the phase transformation, results in a volumetric eigenstrain within the martensitic phase while the lattice shear during the transformation yields an eigenshear component ε^0_{12}. For the same load applied, the eigenstrain leads to higher tensile stresses in vertical direction at the crack tip while compressive stress is induced in the adjacent austenitic area below the crack and the martensitic phase.

Consequentially, the crack does not propagate straight through the specimen but kinks and grows initially in vertical direction (Fig. 4b). Additionally, it can be observed that the crack propagation does not start until the martensitic phase has grown almost completely through the specimen (Fig. 4b). Generally, the martensitic transformation dissipates energy, which is therefore not available for cracking (see [2]). When the martensitic plate extends across the width of the specimen, the elastic energy, which arises due to the eigenstrain, can be reduced on the macro level in that the specimen is deformed (see [22]). Yet, this deformation of the specimen induces additional stress on the crack tip. Regarding the considered eigenstrain tensor $\boldsymbol{\varepsilon}_0$ in (30), the shear component ε^0_{12} is considerably larger than the volumetric components $\varepsilon^0_{\mathrm{vol}}$, leading to a shear loading when the martensitic phase has grown through the specimen. This shear loading induces high normal stresses in horizontal direction below the crack tip in the martensitic phase (Fig. 6b).

The crack starts to propagate perpendicular to the strain axis in vertical direction. Short cracks in metastable austenitic steels, which are oriented perpendicular to the strain axis have been experimentally observed, e.g., by [2].

During the next time steps, the crack proceeds to propagate in the transition zone between the phases. Considering the phase field potential for martensitic transformations in (3), the contributions of the gradient energy density ψ^{grad} and the separation energy density ψ^{sep} are high in the transition zone. These energy contributions can be reduced by the crack propagating in the phase boundary. In experimental studies, cracks propagating along austenite-austenite grain boundaries are observed (see, e.g. [2]). For boundary orientations, which deviate strongly from the current crack propagation direction, Stolarz and coworkers find a temporal crack stopping. For this example, the interface between the phases exhibits a strong curvature. However, the expansion of the martensitic phase in vertical direction enables the crack to grow in the transition zone without strong changes in direction. Therefore, the crack formation also has impact on the evolution of α'-martensite.

Subsequently, the α'-martensite continues expanding in such a way that the crack propagates vertically within the α'-phase (Fig. 4c). This again coincides with the findings in [2], where the authors observe the crack growing without reaching the austenite-α'-martensite boundary.

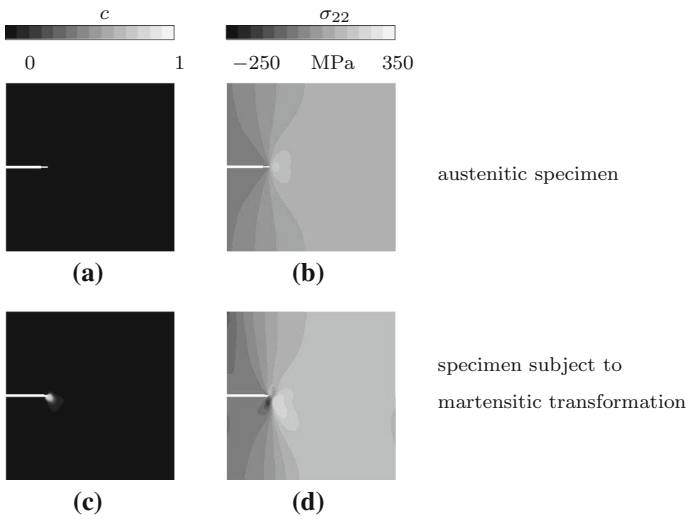

Fig. 5 Contour plots of σ_{22}-components (*right*) and the corresponding evolution of the martensitic phase (*left*, austenite: *white*, martensite: *black*), first row: austenitic specimen, second row: specimen subject to phase transformation. **a** $t = 1.5\,10^{-7}$. **b** $t = 1.5\,10^{-7}$. **c** $t = 1.5\,10^{-7}$. **d** $t = 1.5\,10^{-7}$

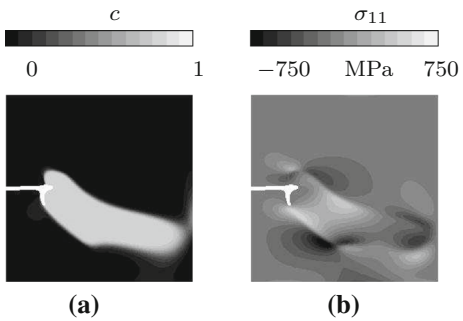

Fig. 6 Contour plot of σ_{11}-component (*right*) and the corresponding evolution of the martensitic phase (it left, austenite: *white*, martensite: *black*). **a** $t = 2.17\,10^{-7}$. **b** $t = 2.17\,10^{-7}$

It can be concluded that the martensitic formation influences the crack propagation and vice versa. Thereby, the eigenstrain within the α'-martensite affects the process on the microscale strongly. The simulation results could be related to experimental observations.

5 Summary

A combined phase field model for martensitic transformations and fracture is proposed, based on the damage variable $s \in [0, 1]$, which is assumed to evolve according to the TDGL equation. The damage variable is combined with the model for martensitic transformations introduced in [22,23] to study the impact of the martensitic transformation on the crack propagation. In accordance with experimental observations α'-martensite forms at the crack tip, which clearly influences the crack path. Due to the volume change and the lattice distortion during the phase transformation, an eigenstrain in the martensitic phase arises. This leads to a different stress field compared to a homogeneous austenitic specimen with the same load applied. The eigenstrain induces a shear deformation, which initiates the crack propagation.

For future work, the influence of microstructure, especially the phase properties on the crack formation, will be investigated, where, e.g., the eigenstrain, the energy barrier and the velocity of the phase transformation could be taken into account.

Acknowledgments This work was financially supported by the Deutsche Forschungsgemeinschaft, SFB 926.

References

1. Khan, Z., Ahmed, M.: Stress-induced martensitic transformation in metastable austenitic stainless steels: effect on fatigue crack growth rate. J. Mater. Eng. Perform. **5**(2), 201–208 (1996)
2. Stolarz, J., Baffie, N., Magnin, T.: Fatigue short crack behaviour in metastable austenitic stainless steels with different grain sizes. Mater. Sci. Eng. A **319–321**, 521–526 (2001)
3. Nebel, T., Eifler, D.: Cyclic deformation behaviour of austenitic steels at ambient and elevated temperatures. Sadhana **28**, 187–208 (2003)
4. Roth, I., Krupp, U., Kübbeler, J.C.H.M., Fritzen, C.P.: Deformation induced martensite formation in metastable austenitic steel during in situ fatigue loading in a scanning electron microscope. ESOMAT **06030** (2009). doi:10.1051/esomat/200906030
5. Skorupski, R., Smaga, M., Eifler, D., Schmitt, R., Müller, R.: Influence of morphology of deformation induced α-martensite on stress-strain response in a two phase austeniticmartensitic-steel. Key Eng. Mater. **592–593**, 582–585 (2014)
6. Francfort, G., Marigo, J.J.: Revisiting brittle fracture as an energy minimization problem. J. Mech. Phys. Solids. J. Mech. Phys. Solids **46**, 131942 (1998)
7. Bourdin, B.: Numerical implementation of the variational formulation for quasi-static brittle fracture. Interfaces Free Bound. **9**, 411430 (2007). doi:10.4171/IFB/171
8. Bourdin, B., Francfort, G., Marigo, J.J.: The variational approach to fracture. J. Elast. **91**, 5–148 (2008)
9. Kuhn, C., Müller, R.: A continuum phase field model for fracture. Eng. Fract. Mech. **77**, 3625–3634 (2010)
10. Chen, L.Q., Wang, Y., Khachaturyan, A.G.: Kintetics of tweed and twin formation during an ordering transition in a substitutional solid solution. Philos. Mag. Lett. **65**, 15–23 (1992)
11. Wang, Y., Khachaturyan, A.G.: Three-dimensional field model and computer modeling of martensitic transformations. Acta Mater. **2**, 759–773 (1997)
12. Artemev, A., Wang, Y., Khachaturyan, A.G.: Three-dimensional phase field model and simulation of martensitic transformation in multilayer systems under applied stresses. Acta Mater. **48**, 2503–2518 (2000)
13. Jin, Y.M., Artemev, A., Khachaturyan, A.G.: Three-dimensional phase field model of low-symmetry martensitic transformation in polycrystal: simulation of ζ_2'-martensite in aucd alloys. Acta Mater. **49**, 2309–2320 (2001)
14. Levitas, V.I., Lee, D.W., Preston, D.L.: Interface propagation and microstructure evolution in phase field models of stress-induced martensitic phase transformations. Int. J. Plast. **26**, 395–422 (2009)
15. Yamanaka, A., Takaki, T., Tomita, Y.: Elastoplastic phase-field simulation of self- and plastic accommodations in cubic $\rightarrow$ tetragonal martensitic transformation. Mater. Sci. Eng. A **491**, 378–384 (2008)
16. Kundin, A., Raabe, D., Emmerich, H.: A phase-field model for incoherent martensitic transformations including plastic accomodation process in the austenite. J. Mech. Phys. Solids **59**, 2082–2102 (2011)
17. Hildebrand, F., Miehe, C.: Variational phase field modeling of laminate deformation microstructure in finite gradient crystal plasticity. Proc. Appl. Math. Mech. **12**, 37–40 (2012)
18. Gao, L.T., Feng, X.Q., Gao, H.: A phase field method for simulating morphological evolution of vesicles in electric fields. J. Comput. Phys. **228**, 41624181 (2009)
19. Suiker, A.J.S., Turteltaub, S.: Crystalline damage development during martensitic transformations. In: ECOMAS CFD (2006)
20. Garion, C., Skoczen, B.: Combined model of strain-induced phase transformation and orthotropic damage in ductile materials at cryogenic temperatures. Int. J. Damage Mech. **12**, 331–356 (2003)
21. Xu, B.X., Schrade, D., Gross, D., Mueller, R.: Fracture simulation of ferroelectrics based on the phase field continuum and a damage variable. Int. J. Fract. **166**, 163–172 (2010)
22. Schmitt, R., Müller, R., Kuhn, C., Urbassek, H.M.: A phase field approach for multivariant martensitic transformations of stable and metastable phases. Arch. Appl. Mech. **83**, 849–859 (2013)
23. Schmitt, R., Wang, B., Urbassek, H.M., Müller, R.: Modeling of martensitic transformations in pure iron by a phase field approach using information from atomistic simulation. Technische Mechanik **33**, 119–130 (2013)
24. Amor, H., Marigo, J.J., Maurini, C.: Regularized formulation of the variational brittle fracture with unilateral contact: numerical experiments. J. Mech. Phys. Solids **57**, 1209–1229 (2009)
25. Kuhn, C., Müller, R.: Phase field simulation of thermomechanical fracture. Proc. Appl. Math. Mech. **9**, 191–192 (2009)
26. Kuhn, C., Schlüter, A., Müller, R.: A phase field approach for dynamic fracture. Proc. Appl. Math. Mech. **13**, 87–88 (2013)
27. Hofacker, M., Miehe, C.: Continuum phase field modeling of dynamic fracture: variational principles and staggered fe implementation. Int. J. Fract. **178**, 113–129 (2012)
28. Schrade, D., Xu, B.X., Müller, R., Gross, D.: On phase field modeling of ferroelectrics: parameter identification and verification. SMASIS **1**, 299–306 (2008)
29. Schrade, D., Mueller, R., Xu, B., Gross, D.: Domain evolution in ferroelectric materials: a continuum phase field model and finite element implementation. Comput. Methods Appl. Mech. Eng. **196**, 4365–4374 (2007)
30. Du, Q., Liu, C., Wang, X.: A phase field approach in the numerical study of the elastic bending energy for vesicle membranes. J. Comput. Phys. **198**, 450468 (2004)
31. Wechsler, M.S., Lieberman, D.S., Read, T.A.: On the theory of the formation of martensite. J. Metals. Nov. 1503–1515 (1953)
32. Schmitt, R., Kuhn, C., Müller, R., Bhattacharya, K.: Crystal plasticity and martensitic transformations—a phase field approach. Technische Mechanik **34**, 23–28 (2014)